EUROPEAN ORGANIZATION FOR NUCLEAR RESEARCH

CERN-EP/80-81
30 May 1980

A PARTIAL WAVE ANALYSIS OF DIFFRACTIVELY PRODUCED $\bar{\Lambda}p$ AND $\Lambda\bar{p}$ STATES

W.E. Cleland[a], A. Delfosse[b], P.A. Dorsaz[b], J.L. Gloor[c],
M.N. Kienzle-Focacci[b], G. Mancarella[b], A.D. Martin[d],
M. Martin[b], P. Mühlemann[b], C. Nef[b], T. Pal[b],
J. Rutschmann[b] and H. Zeidler[c]

a University of Pittsburgh, Pittsburgh, PA, USA
b Université de Genève, Geneva, Switzerland
c Université de Lausanne, Lausanne, Switzerland
d University of Durham, Durham, UK

ABSTRACT

In a study of the $\bar{\Lambda}p$ and $\Lambda\bar{p}$ systems, produced in the reactions $K^+p \to (\bar{\Lambda}p)p$ and $K^-p \to (\Lambda\bar{p})p$ at 50 GeV/c, we find evidence for three broad states with unnatural parity $J^\eta = 2^-$, 3^+, and 4^-, centred at 2.26, 2.32, and 2.49 GeV, respectively.

(Submitted to Nuclear Physics B)

1. INTRODUCTION

This is a study of the $\bar{\Lambda}p$ and $\Lambda\bar{p}$ systems, produced diffractively in the reactions $K^+p \to (\bar{\Lambda}p)p$ and $K^-p \to (\Lambda\bar{p})p$, respectively. The data sample consists of 3368 events of the K^+-initiated reaction and 2709 events of the K^- one. It has been obtained with the Geneva-Lausanne spectrometer at the CERN SPS, at an incident beam momentum of 50 GeV/c [1]. The set-up was similar to the one used in a previous experiment at 10 GeV/c at the CERN PS, which is described in detail elsewhere [2]. A first analysis of the data has been published previously [3]. There we found that the moments of the decay $R^+ \to \bar{\Lambda}p$ and $R^- \to \Lambda\bar{p}$ exhibit very significant structure, in particular the terms $N(Y_L^0)$ with L = 4, 6, and 8. We have interpreted the moments in terms of a simple model, consisting of two unnatural-parity states, a $J^\eta = 2^-$ state at 2.3 GeV and a 4^- state at 2.5 GeV, and a smooth 0^- background.

Here we use the double moments of the sequential decay $R^+ \to \bar{\Lambda}p$, $\bar{\Lambda} \to \bar{p}\pi^+$ (and its charge conjugate) to perform an amplitude analysis which is to a large extent model independent [4]. We find the additional information on the polarization of the $\bar{\Lambda}$, as measured by the asymmetry in its parity-violating decay, provides strong constraints on the partial waves of the $\bar{\Lambda}p$ system. This allows us to confirm the previously found even spin states, as well as to investigate the mass structure of the odd spin states with unnatural parity $J^\eta = 1^+$ and 3^+.

2. DOUBLE MOMENTS

We use the data to study the production of mesonic states R by the processes $K^\pm p \to R^\pm p$, and their subsequent decay $R^+ \to \bar{\Lambda}p$, $\bar{\Lambda} \to \bar{p}\pi^+$, and $R^- \to \Lambda\bar{p}$, $\Lambda \to p\pi^-$. For a detailed discussion of the formalism describing such sequential decays see the preceding paper [4].

The double moments are defined as follows:

$$H(LM\ell m) \equiv \sum_{i=1}^{N} w_i D^L_{Mm}(\phi_i,\theta_i,0) D^{\ell}_{mo}(\phi_{1i},\theta_{1i},0) \ , \qquad (1)$$

where θ_i,ϕ_i are the $\bar{\Lambda}$ angles of event i in the decay $R^+ \to \bar{\Lambda}p$, and θ_{1i},ϕ_{1i} are the $\bar{p}$ angles in the decay $\bar{\Lambda} \to \bar{p}\pi^+$. The reference frame is shown in fig. 1 (t-channel

helicity frame for R^+). The weights w_i have been determined by Monte Carlo calculations in order to correct for geometrical acceptance, detector inefficiency, and other losses. The sum is over all events in a given bin of $\bar{\Lambda}p$ mass. Figures 2 to 4 show the non-zero moments as a function of $\bar{\Lambda}p$ mass, integrated over the momentum-transfer range $0.05 < -t < 1$ $(GeV/c)^2$.

The moments H(LM00) describe the angular distribution of the R decay and are directly related to the simple moments $N\langle Y_L^M\rangle$ of Ref. 3 by $H(LM00) = N\langle Y_L^M\rangle/\sqrt{2L+1}$. They are real. Figure 2 shows the moments H(L000), which are used in the present analysis*). As both K^+- and K^--initiated data show very similar structure, the two data sets have been added in fig. 2. Notice in particular the broad, very significant peaks in L = 4, 6, and 8, which we reported in our previous publication [3]. The moments with $M \neq 0$ (not shown) are strongly suppressed with respect to M = 0; we find that $H(L100) \lesssim 0.3\ H(L000)$.

The moments with $\ell = 1$ and $m = 0, \pm 1$ are related to the components of the $\bar{\Lambda}$ polarization vector $\vec{P}$ times the asymmetry parameter α which characterizes the parity violation in weak $\bar{\Lambda}$ decay. These moments are pure imaginary. It is convenient to use the combinations H(LM11) + H(LM1-1), H(LM11) - H(LM1-1), and H(LM10), which are proportional, for M = 0, to P_x, P_y, and P_z respectively.

Owing to CP conservation $\alpha_{\bar{\Lambda}} = -\alpha_{\Lambda}$, so that we expect all $\ell = 1$ moments to change sign when going from the K^+- to the K^--initiated reactions. We have assumed that $\vec{P}_{\bar{\Lambda}} = \vec{P}_{\Lambda}$. This property is evident in the data, and is illustrated by fig. 3 in the case of H(1011) - H(101-1). Apart from this sign change we find the structure of the polarization moments to be the same in both reactions. For this reason we have combined the data by inverting the sign of the p-direction in the K^--initiated reaction.

The combined polarization moments H(L011) - H(L01-1) are shown in fig. 4. We find no significant signal in any $\ell = 1$ moment with $M \neq 0$. Recall that the other $\ell = 1$ moments, H(L011) + H(L01-1) and H(L010), must vanish [4], i.e. the $\bar{\Lambda}$ can only

---

*) Small differences with respect to the data in Ref. 3 can be attributed to an improved method of acceptance correction taking into account the Λ-decay asymmetry.

be transversely polarized, normal to the plane containing the momentum vectors of the $\bar{\Lambda}$ and the incident K^+. Figure 4 shows a very large, broad signal in L = 1, implying that polarization effects are indeed important in these reactions. Smaller signals appear in L = 5 and 7.

It is very striking that most of the significant structures appear in H(L000) moments with L even, and in H(L011) - H(L01-1) moments with L odd. This fact has to be accounted for by production amplitudes.

3. AMPLITUDE ANALYSIS

The production of a state R with spin-parity $A \equiv J^\eta$ and helicity Λ can be described by an amplitude H^A_Λ. It is convenient to use the linear combinations of amplitudes describing (in the high-energy limit) production by natural-parity exchange (NPE) and unnatural-parity exchange (UPE), which we denote by N^A_Λ and U^A_Λ, respectively:

$$N^A_\Lambda = C_\Lambda\left[H^A_\Lambda - \sigma(-1)^\Lambda H^A_{-\Lambda}\right]$$
$$U^A_\Lambda = C_\Lambda\left[H^A_\Lambda + \sigma(-1)^\Lambda H^A_{-\Lambda}\right] \qquad C_\Lambda = \begin{cases} 1/2 & \text{for } \Lambda = 0 \\ 1/\sqrt{2} & \text{for } \Lambda \neq 0 \end{cases} \qquad (2)$$

where $\sigma = \eta(-1)^J$ is the naturality of the produced state. At 50 GeV/c incident momentum it is reasonable to assume that NPE dominates. The observed dominance of the M = 0 moments means that the $\bar{\Lambda}p$ system is mainly produced with helicity $\Lambda = 0$. This then implies that the spin-parity of the system is of the unnatural series $J^\eta = 0^-, 1^+, 2^- \ldots$ [3,4].

The decay $R^+ \to \bar{\Lambda}p$ is characterized by an amplitude $F^A_{\lambda_1\lambda_2}$, where λ_1, λ_2 are the helicities of the two baryons in the final state. There are two independent amplitudes, F^A_{++} (non-flip) and F^A_{+-} (flip). For unnatural-parity states A, these correspond to the spin-singlet and the spin-triplet configuration of the $\bar{\Lambda}p$ system in the L-S formalism.

The generalization of C-parity conservation within SU(3) leads to the selection rule J + S = even, where S is the spin-configuration of the $\bar{\Lambda}p$ system [3,4]. Even J states are therefore spin-singlets, while odd J states are spin-triplets.

In our analysis we therefore consider only the following over-all production and decay amplitudes:

$$\text{and} \qquad \begin{aligned} J_0^{++} &\equiv N_0^{A\bar{A}} F_{++}^{A} \quad \text{for J even} \\ J_0^{+-} &\equiv N_0^{A\bar{A}} F_{+-}^{A} \quad \text{for J odd .} \end{aligned} \tag{3}$$

As we observe significant signals in the moments up to L = 8, we attempt to describe the data by S_0^{++}, P_0^{+-}, D_0^{++}, F_0^{+-}, and G_0^{++}. Notice that the s- and p-wave amplitudes describing the decay $\bar{\Lambda} \to \bar{p}\pi^+$, which interfere to give the asymmetry parameter α, are known. The asymmetry parameter is included in the coefficients listed in eqs. (5), where we use $\alpha_{\bar{\Lambda}} = -0.642$.

The moments H(L000) can be expanded as linear combinations of amplitude products of the type Re $(J_0^{++} J_0'^{++*})$ and Re $(J_0^{+-} J_0'^{+-*})$, where the two amplitudes are either both non-flip or both flip. In contrast, the polarization moments H(L011) - - H(L01-1) arise from interference between a non-flip and a flip amplitude, involving terms of the type Im $(J_0^{++} J_0'^{+-*})$. As a consequence, our model [eq. (3)] predicts H(L000) = 0 for L odd, and H(L011) - H(L01-1) = 0 for L even. This is to a large extent verified by the data. An exception is the small, but statistically significant value of H(1000) and H(3000), which cannot be explained in the framework of this model. A detailed discussion of the general relations between moments and amplitudes is given elsewhere [4]. Here it suffices to list the explicit expressions used to confront the data; the single moments are

$$\begin{aligned} H(0000) &= 2|S_0|^2 + 2|P_0|^2 + 2|D_0|^2 + 2|F_0|^2 + 2|G_0|^2 \\ H(2000) &= 1.789 S_0 D_0 - 0.400|P_0|^2 + 1.283 P_0 F_0 + 0.571|D_0|^2 + \\ &\quad + 1.533 D_0 G_0 + 0.400|F_0|^2 + 0.519|G_0|^2 \\ H(4000) &= 1.333 S_0 G_0 - 0.713 P_0 F_0 + 0.571|D_0|^2 + 0.774 D_0 G_0 + \\ &\quad + 0.061|F_0|^2 + 0.324|G_0|^2 \\ H(6000) &= 0.938 D_0 G_0 - 0.350|F_0|^2 + 0.280|G_0|^2 \\ H(8000) &= 0.403|G_0|^2 \end{aligned} \tag{4}$$

and the polarization moments are given by the following expressions:

$$\begin{aligned}
\text{Im}\left[H(1011) - H(101\text{-}1)\right] &= 0.699S_0P_0 + 0.313P_0D_0 + 0.501D_0F_0 + 0.374F_0G_0 \\
\text{Im}\left[H(3011) - H(301\text{-}1)\right] &= 0.458S_0F_0 - 0.328P_0D_0 + 0.245P_0G_0 + 0.205D_0F_0 - \\
&\quad - 0.042F_0G_0 \qquad (5) \\
\text{Im}\left[H(5011) - H(501\text{-}1)\right] &= - 0.246P_0G_0 + 0.294D_0F_0 - 0.111F_0G_0 \\
\text{Im}\left[H(7011) - H(701\text{-}1)\right] &= - 0.242F_0G_0 \ .
\end{aligned}$$

Here we have dropped the helicity superscripts, and used the abbreviation J_0J_0' to denote Re $(J_0J_0'^*)$ in eqs. (4) and to denote Im $(J_0J_0'^*)$ in eqs. (5).

In all such amplitude products there is an implicit summation of nucleon spin-flip and non-flip at the lower vertex of the production process. Under the assumption of nucleon spin coherence [4] the interference terms can be rewritten in the form

$$\begin{aligned}
\text{Re}\ (J_0J_0'^*) &= |J_0|\ |J_0'|\ \cos\phi_{JJ'} \\
\text{Im}\ (J_0J_0'^*) &= |J_0|\ |J_0'|\ \sin\phi_{JJ'}\ ,
\end{aligned} \qquad (6)$$

where $\phi_{JJ'}$ is the relative phase between amplitudes J_0 and J_0'. It can be decomposed into

$$\phi_{JJ'} = \theta_J + \delta_J - \theta_{J'} - \delta_{J'}\ , \qquad (7)$$

where θ_J is the production and δ_J the decay phase of the spin J amplitude.

We are thus left with 5 amplitude magnitudes and 4 relative phases, to be determined from 9 observables, by solving the system of eqs. (4) and (5) in each mass bin independently.

All the solutions of this system have been generated in each bin by using the technique of Barrelet zeros [5]. The method is the same as the one employed in the analysis of the reaction $\bar{p}p \to \pi\pi$ [6]. One considers the "transversity" amplitude

$$\begin{aligned}
T(\theta) &= \sum_{J\ \text{even}} \sqrt{\frac{2J+1}{4\pi}}\ J_0^{++}P_J(\cos\theta) - i \sum_{J\ \text{odd}} \sqrt{\frac{2J+1}{4\pi}}\ \frac{1}{\sqrt{J(J+1)}}\ J_0^{+-}P_J^1(\cos\theta) \equiv \\
&\equiv T^{++}(\theta) - i\ T^{+-}(\theta)\ ,
\end{aligned} \qquad (8)$$

which is related to the angular distribution and polarization of the $\bar{\Lambda}$ by

$$W(\Omega) = |T^{++}|^2 + |T^{+-}|^2$$
$$Py(\Omega)W(\Omega) = -2\ \mathrm{Im}\ (T^{++}T^{+-*}) \ . \tag{9}$$

By substituting a complex $\omega \equiv e^{i\theta}$ for cos θ and sin θ, we can rewrite T as a polynomial of degree 2n in ω, and factorize in terms of its roots ω_i

$$T(\omega) = \frac{1}{\omega^n}\prod_{i=1}^{2n}(\omega-\omega_i) = \frac{1}{\omega^n}\prod_{i=1}^{n}(\omega-\omega_i)(\omega+1/\omega_i) \ , \tag{10}$$

where $n = J_{max} = 4$. The second part of eq. (10) is a consequence of our specific model eq. (3): the 2n roots group themselves in n pairs ω_i, $-1/\omega_i$.

In fig. 5 we show the location of the roots ω_i as a function of $\bar{\Lambda}p$ mass. We have drawn the member with Re $\omega_i \geq 0$ of each of the four pairs of roots.

The transformation of any pair

$$(\omega_i, -1/\omega_i) \rightarrow (1/\omega_i^*, -\omega_i^*) \tag{11}$$

leaves the observables, eq. (9), unchanged, but does change the amplitudes. With n pairs, we thus obtain 2^n solutions. Since half of these are just complex conjugates of the other half, we obtain $2^{n-1} = 8$ distinct solutions in each mass bin. Each solution is then traced from bin to bin by using the trajectories shown in fig. 5.

4. DISCUSSION OF THE RESULTS

The results of solving eqs. (4) and (5) are illustrated by figs. 6 and 7. We have imposed correct threshold behaviour by drawing smooth curves $\sim p^L$ through the moments L = 5, 6 for M < 2.24 GeV and through L = 7, 8 for M < 2.36 GeV. We find that the structure of the amplitude magnitudes is very similar in all 8 solutions. They all show broad peaks in $|D_0|$, $|F_0|$, and $|G_0|$ in the mass region 2.3-2.5 GeV. This common feature is illustrated by the particular solution shown in fig. 6. The main differences occur in the less well determined S_0 and P_0 amplitudes. The structure of these lower waves, in particular the peak in $|P_0|$ near threshold, is solution dependent. A fit of a relativistic Breit-Wigner amplitude to $|D_0|$, $|F_0|$,

and $|G_0|$ gives the parameters listed in table 1. The width of the 3^+ and 4^- states is not well determined from the data and has been fixed in the fit. The errors on the cross-sections include systematic uncertainties; the errors on the mass and width parameters indicate the dispersion among the different solutions.

The relative phases are solution dependent. Common to all solutions is, however, some phase variation as a function of mass. The particular solution shown in fig. 7 is compared with expectations for Breit-Wigner phases for the D_0, F_0, and G_0 waves (dotted lines). The phase of the S_0 and P_0 waves has been assumed to be constant. For this solution the relative phases are in good agreement with Breit-Wigner resonances and, moreover, show evidence of a common phase, θ_J, for resonance production in $K^-p \to R^-p$ *). The assumption of a constant P_0 wave phase is in contradiction with the data at low mass, as could be anticipated from the behaviour of $|P_0|$ in fig. 6.

In fig. 8 we compare the strange mesonic states with natural and unnatural parity on a Chew-Frautschi plot. The new 2^-, 3^+, and 4^- states lie, well below the natural-parity K^* resonances, in the neighbourhood of the curve $J = pR$, with $p = \Lambda$ momentum in the c.m. and $R = 1$ fm. Above this curve, the excitation of resonances in the $\bar{\Lambda}p$ channel is kinematically suppressed.

We notice that recent amplitude analyses of the $\bar{p}p$ system in both formation [6] and production [7] experiments show evidence for a similar, rich spectrum of broad resonances below the leading trajectory. These non-strange mesons, however, couple to $\pi\pi$ and thus are of the natural-parity series $J^\eta = 2^+, 3^-, 4^+ \ldots$.

5. CONCLUSIONS

Our analysis of the production of mesonic states $R^\pm$ with strangeness $S = \pm 1$ in the reaction $K^\pm p \to R^\pm p$ and of their sequential decay $R^+ \to \bar{\Lambda}p$, $\bar{\Lambda} \to \bar{p}\pi^+$ (and charge conjugate) by means of double moments confirms the important structures in the moments up to $L = 8$ which we have reported previously [3]. In addition, the moments which are sensitive to the asymmetry of the $\bar{\Lambda}$ decay show that the $\bar{\Lambda}$ has a large

*) Figure 7, which refers to $K^+p \to R^+p$, indicates that D_0, $-F_0$, and G_0 have, to a good approximation, a common production phase.

transverse polarization. This additional information allows us to determine, in addition to S_0^{++}, D_0^{++} and G_0^{++}, also P_0^{+-} and F_0^{+-} amplitude magnitudes and relative phases. The observed $\bar{\Lambda}$ polarization is due to interference of even and odd waves.

The mass dependence of the amplitude magnitudes gives evidence for three broad states with unnatural parity $J^{\eta} = 2^-$, 3^+, and 4^-. This structure is very similar in all 8 partial wave solutions generated with the Barrelet zero technique. The behaviour of the relative phases is solution dependent, but the data are consistent with Breit-Wigner phases. The interpretation of these new states as resonances provides therefore a natural explanation of all the data.

REFERENCES

[1] W.E. Cleland et al., Phys. Lett. 86B (1979) 409.

[2] R. Baldi et al., Nucl. Phys. B134 (1978) 365.

[3] W.E. Cleland et al., Phy. Lett. 89B (1980) 290.

[4] A.D. Martin and C. Nef, preceding paper.

[5] E. Barrelet, Nuovo Cimento 8A (1972) 331.

[6] A.D. Martin and M.R. Pennington, Phys. Lett. 86B (1979) 93.

[7] M. Rozanska et al., Nucl. Phys. B162 (1980) 505.

Table 1

Parameters of Breit-Wigner fits

J^{η}	M (GeV)	Γ (GeV)	$\Delta\sigma$ a) (μb)
2^-	2.26 ± 0.02	0.21 ± 0.05	0.58 ± 0.09
3^+	2.32 ± 0.03	0.25	0.54 ± 0.08
4^-	2.49 ± 0.02	0.25	0.28 ± 0.04

a) $\Delta\sigma$ is the cross-section for $2.06 \leq M \leq 2.84$ GeV and $0.05 \leq |t| \leq 1$ $(GeV/c)^2$, and an average of K^+- and K^--initiated reactions.

Figure captions

Fig. 1 : Reference frames for the decay $R^+ \to \bar{\Lambda}p$ and the subsequent decay $\bar{\Lambda} \to \bar{p}\pi^+$. $\hat{p}_{inc}$ and $\hat{p}_{rec}$ are the directions of the incident K^+ and of the recoil p, respectively.

Fig. 2 : Acceptance-corrected moments H(L000) as a function of $\bar{\Lambda}p$ mass. Data from the K^+- and K^--initiated reactions have been combined. The vertical scale represents the cross-section integrated over the momentum-transfer range $0.05 \leq |t| \leq 1$ $(GeV/c)^2$, and averaged over K^+ and K^- reactions.

Fig. 3 : Acceptance-corrected polarization moments Im [H(1011) - H(101-1)], plotted separately for the K^+- and K^--initiated reactions.

Fig. 4 : Acceptance-corrected polarization moments Im [H(L011) - H(L01-1)] for the combined K^+ and K^- data. The cross-section scale is defined as in fig. 2.

Fig. 5 : The trajectories of the amplitude zeros ω_i as a function of $\bar{\Lambda}p$ mass in the complex plane $\omega = e^{i\theta}$.

Fig. 6 : Mass dependence of the amplitude magnitudes. The cross-section scale is defined as in fig. 2.

Fig. 7 : Mass dependence of the relative phases. The dotted lines are expectations from the assumption of resonant Breit-Wigner phases for D_0, $-F_0$, and G_0, and a constant phase for S_0 and P_0. An additional constant phase of 20° has been included in D_0. The phase behaviour is solution dependent. The phases plotted correspond to zeros A, B and C chosen to have $|\omega_i| \geq 1$ and zero D to have $|\omega_i| \leq 1$.

Fig. 8 : Comparison of strange mesons with natural and unnatural parity on a Chew-Frautschi plot. The excitation of resonances above the curve J = pR is kinematically inhibited in the $\bar{\Lambda}p$ channel.

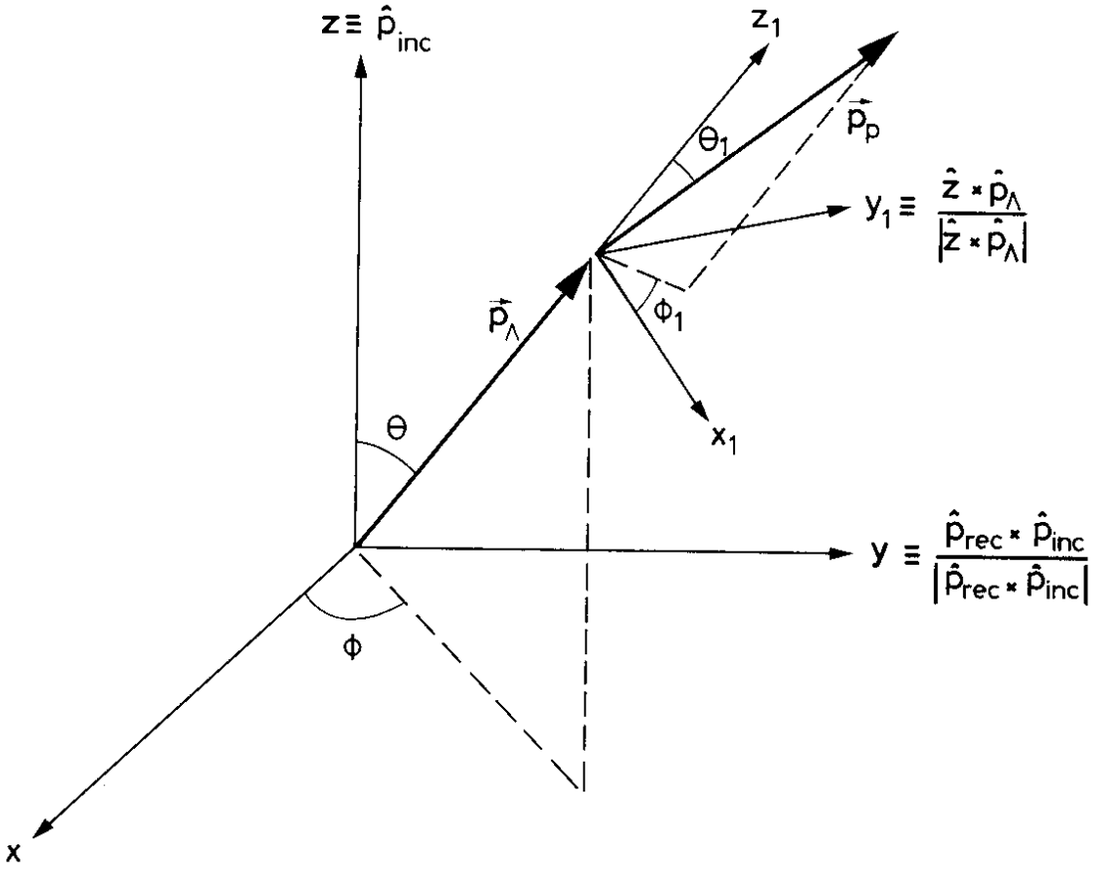

Fig. 1

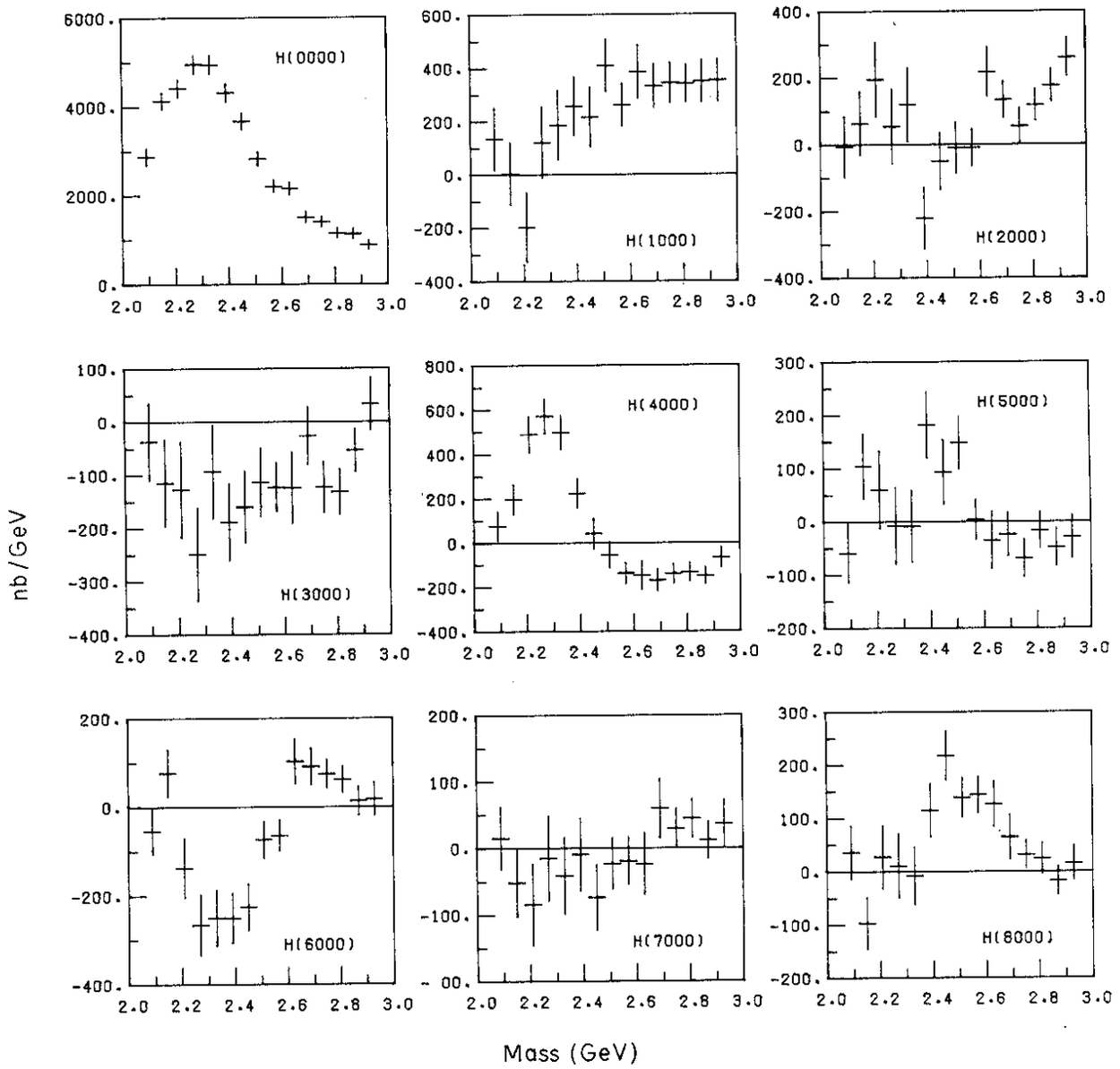
H(0000)
H(1000)
H(2000)
H(3000)
H(4000)
H(5000)
H(6000)
H(7000)
H(8000)
nb/GeV
Mass (GeV)

Fig. 2

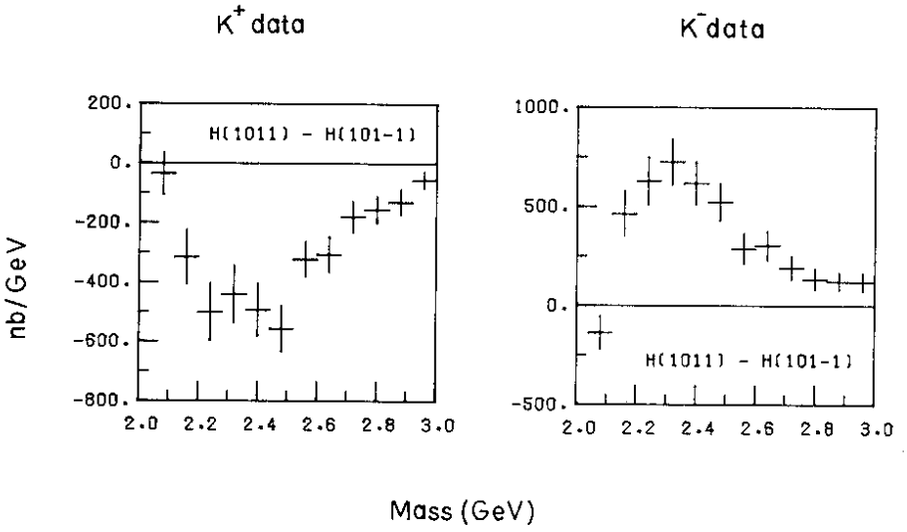
K+ data
K- data
H(1011) - H(101-1)
H(1011) - H(101-1)
nb/GeV
Mass (GeV)
200.
0.
-200.
-400.
-600.
-800.
1000.
500.
0.
-500.
2.0
2.2
2.4
2.6
2.8
3.0

Fig. 3

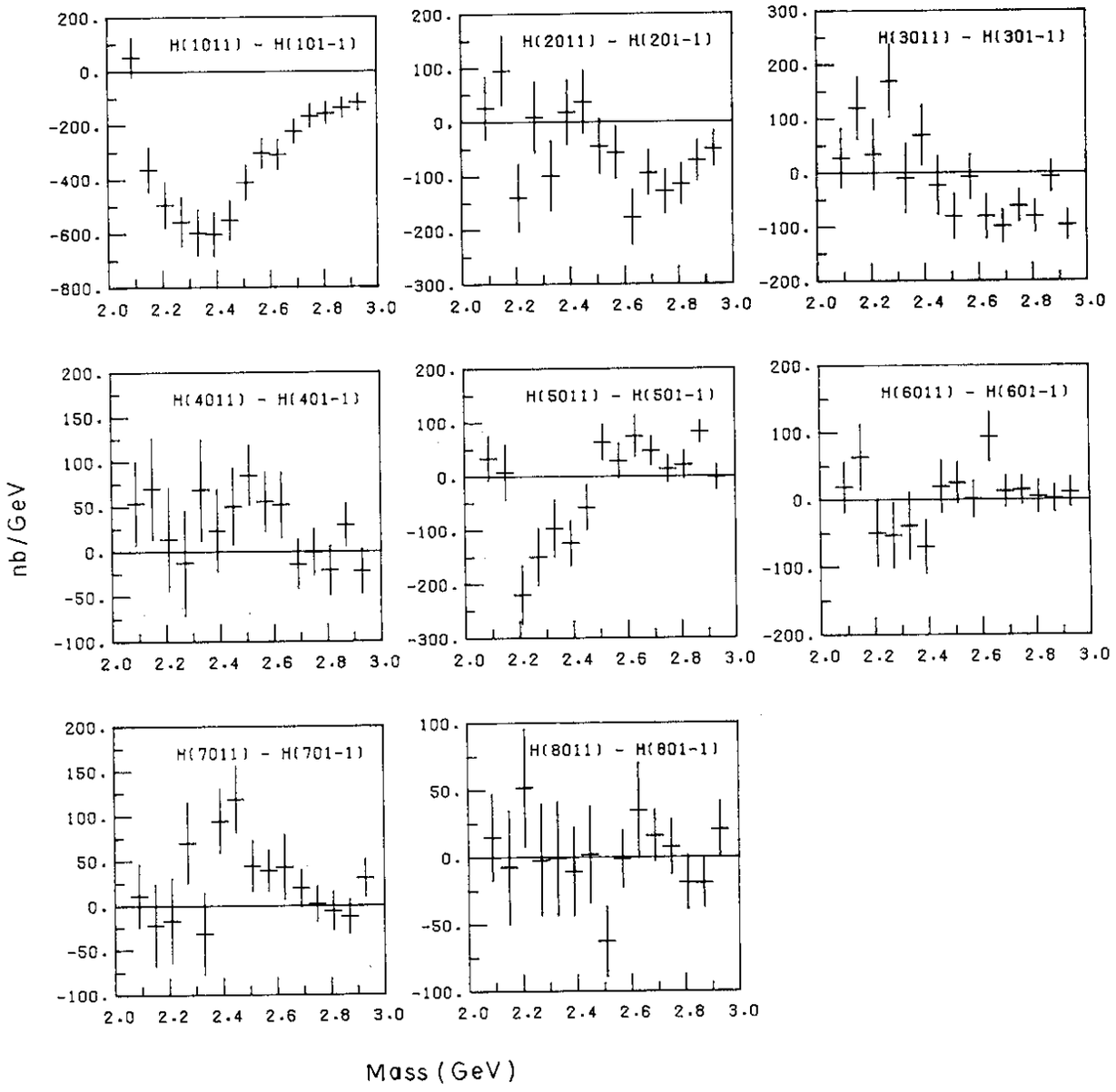
H(1011) - H(101-1)
H(2011) - H(201-1)
H(3011) - H(301-1)
H(4011) - H(401-1)
H(5011) - H(501-1)
H(6011) - H(601-1)
H(7011) - H(701-1)
H(8011) - H(801-1)
nb/GeV
Mass (GeV)

Fig. 4

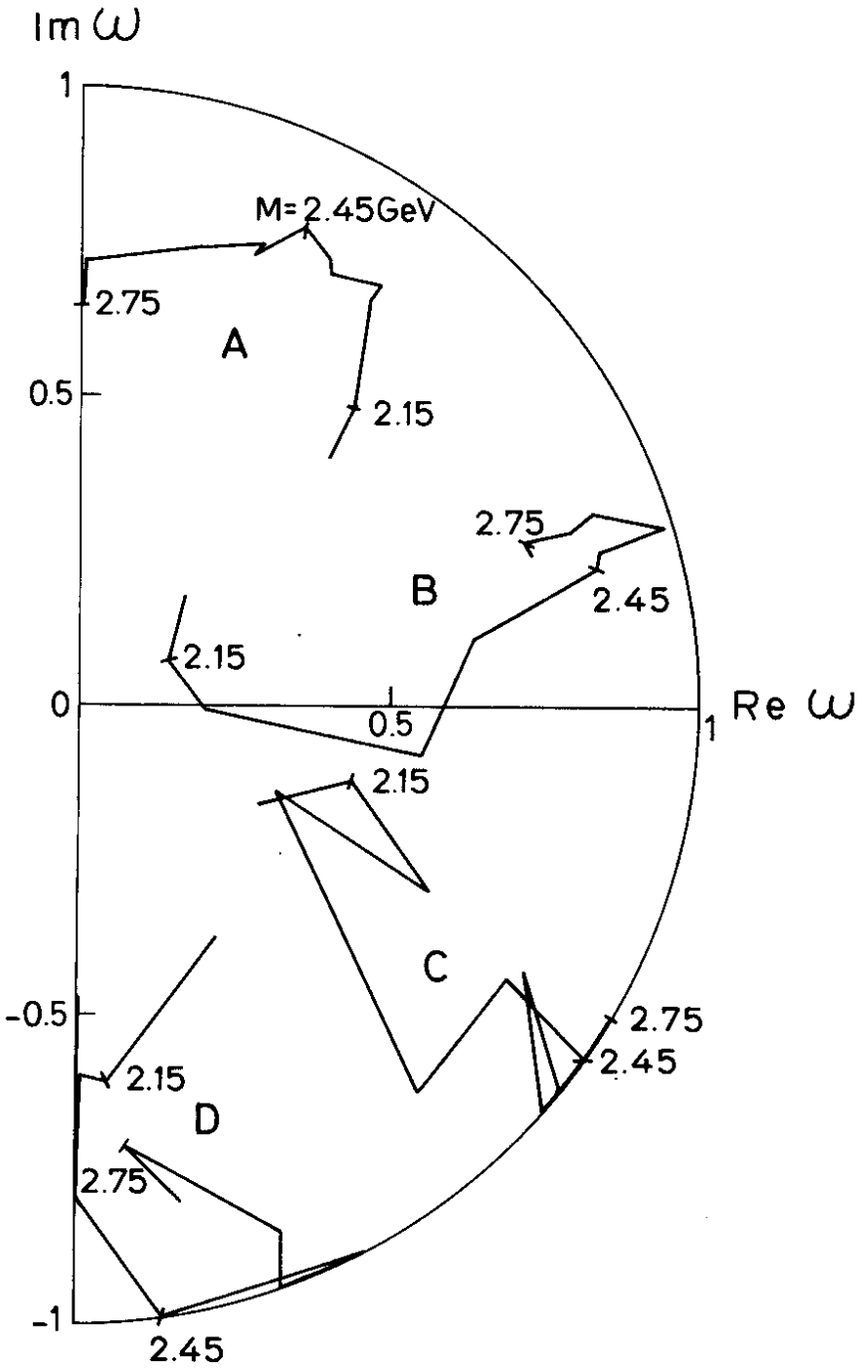
Im ω
1
M=2.45GeV
2.75
A
0.5
2.15
2.75
B
2.45
2.15
0
0.5
1
Re ω
2.15
C
-0.5
2.75
2.45
2.15
D
2.75
-1
2.45

Fig. 5

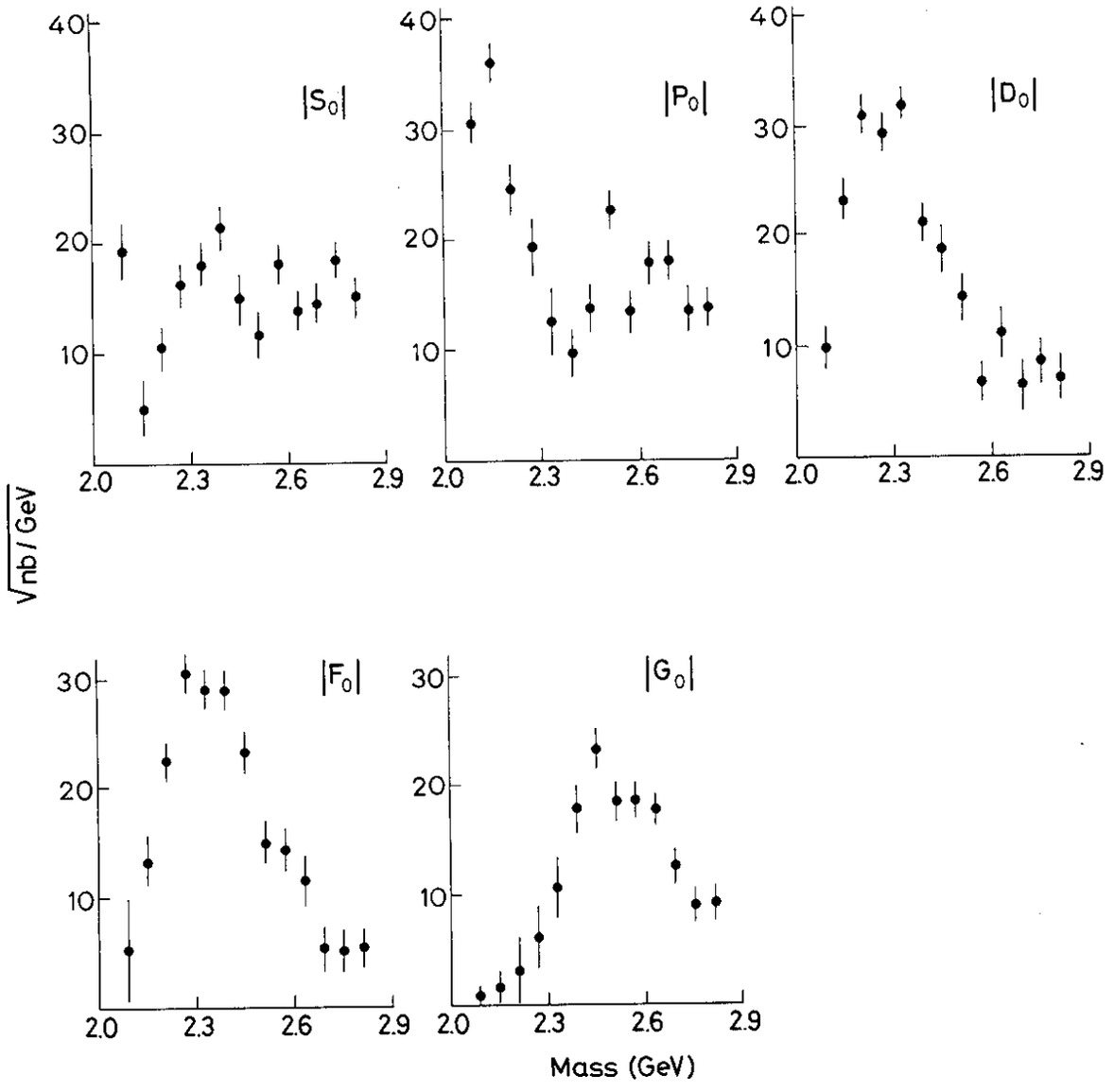

Fig. 6

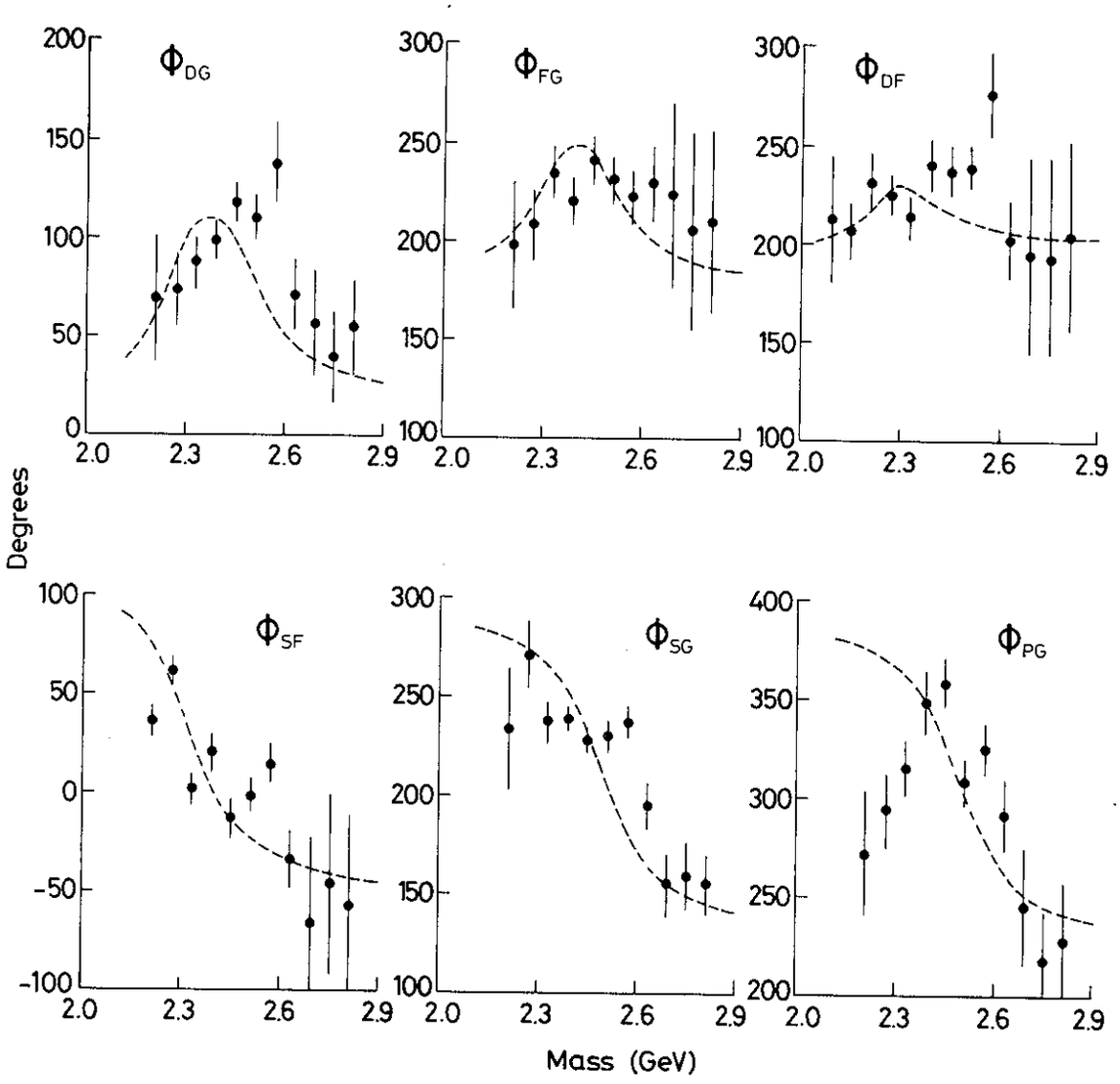

Fig. 7

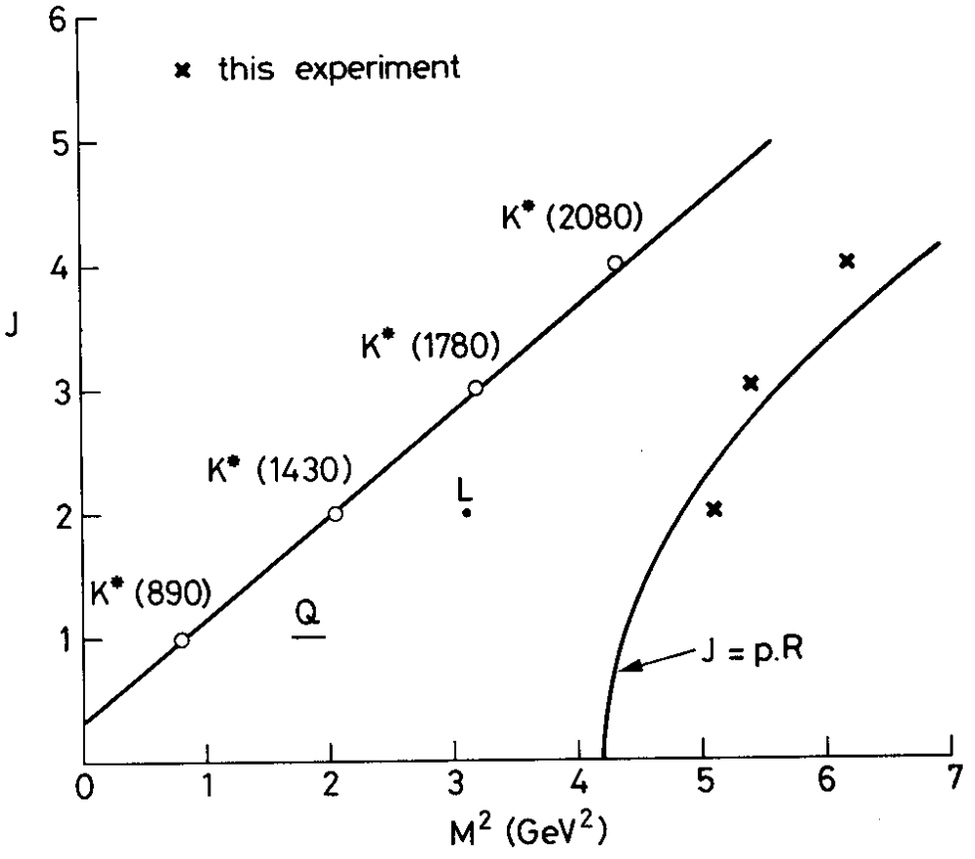
× this experiment
K* (2080)
K* (1780)
K* (1430)
K* (890)
Q
L
J = p.R
J
M² (GeV²)
0
1
2
3
4
5
6
7

Fig. 8